Pure nematic quantum critical point accompanied by a superconducting dome

Kousuke Ishida[a,1,2] , Yugo Onishi[a,3] , Masaya Tsujii[a], Kiyotaka Mukasa[a], Mingwei Qiu[a], Mikihiko Saito[a] , Yuichi Sugimura[a] , Kohei Matsuura[a,3],
Yuta Mizukami[a,4] , Kenichiro Hashimoto[a] , and Takasada Shibauchi[a,2]

When a symmetry-breaking phase of matter is suppressed to a quantum critical point (QCP) at absolute zero, quantum-mechanical fluctuations proliferate. Such fluctuations can lead to unconventional superconductivity, as evidenced by the superconducting domes often found near magnetic QCPs in correlated materials. Experimentally, however, it remains much less clear whether the superconductivity can be promoted around QCPs of the electronic nematic phase, characterized by rotational symmetry breaking. Here, we demonstrate from systematic elastoresistivity measurements that nonmagnetic FeSe$_{1-x}$ Te$_x$ exhibits an electronic nematic QCP showing diverging nematic susceptibility. This finding establishes two nematic QCPs in FeSe-based superconductors with contrasting accompanying phase diagrams. In FeSe$_{1-x}$ Te$_x$, a superconducting dome is centered at the QCP, whereas FeSe$_{1-x}$ S$_x$ shows no QCP-associated enhancement of superconductivity. We find that this difference is related to the relative strength of nematic and spin fluctuations. Our results in FeSe$_{1-x}$ Te$_x$ present the unprecedented case in support of the superconducting dome being associated with the QCP of pure electronic nematic order, which does not intertwine with any other long-range orders.

superconductivity | quantum critical point | electronic nematic state | quantum liquid crystals | phase diagram

In unconventional superconductors, the interplay between superconductivity (SC) and a quantum critical point (QCP), defined as the point of continuous phase transition at absolute zero temperature, has been one of the central topics for decades. At the QCP, the ground state becomes a scale-invariant critical state, in which quantum-mechanical fluctuations are substantially enhanced (1). These enhanced quantum fluctuations couple with the low-energy quasiparticle excitations near the Fermi energy, which causes the non-Fermi liquid power law behavior of the physical quantities and sometimes leads to the formation of Cooper pairs. In particular, the focus of interest has been on the antiferromagnetic QCPs found in many classes of unconventional superconductors, such as heavy-fermion and iron-pnictide superconductors (2, 3). The phase diagrams of these materials show a dome-shaped superconducting phase near the vanishing point of the antiferromagnetic phase, which implies that strong spin fluctuations near the antiferromagnetic QCP can mediate the superconductivity with high critical temperature T_c (4).

In recent years, several kinds of unconventional superconductors have also been found to exhibit electronic nematic orders, which break rotational symmetry of the underlying lattice, close to the superconducting phase (5–7). It is then important to investigate whether such nematic fluctuations can promote unconventional superconductivity or not. Theoretical studies have pointed out that they can enhance the critical temperature T_c (8–10). Indeed, recently, nematic fluctuations in Ba$_{1-x}$ Sr$_x$ Ni$_2$ As$_2$ have been shown to contribute to an increase of T_c (11), and the drastic suppression of T_c under the uniaxial strain in Ba(Fe$_{1-x}$ Co$_x$)$_2$ As$_2$ (12) is in line with the nematicity-mediated superconductivity predicted in the theory (13). However, the nematic orders in these materials coexist with other intertwined spin or charge orders, which makes it challenging to experimentally establish that nematic fluctuations themselves can strengthen the superconducting pairing.

The iron-chalcogenide superconductor FeSe is an ideal system to address this issue. This compound exhibits an electronic nematic phase below the tetragonal to orthorhombic structural transition temperature $T_s \sim 90$ K, but unlike most iron-based superconductors, it does not show any long-range magnetic order down to zero temperature (14). By applying hydrostatic pressure, T_s of FeSe is rapidly suppressed, but before the vanishing of nematic order, a pressure-induced antiferromagnetic order sets in. This magnetic phase shows a dome shape in the pressure phase diagram, whereas T_c exhibits a fourfold increase from 9 K at ambient pressure up to ∼37 K when the antiferromagnetism is suppressed at high pressure (15). In contrast, the isovalent S substitution for Se can suppress T_s to zero

Significance

The notion of
the quantum critical point (QCP) is at the core of modern condensed matter physics. Near a QCP of the symmetry-breaking order, associated quantum-mechanical fluctuations are intensified, which can lead to unconventional superconductivity. Indeed, dome-shaped superconducting phases are often observed near the magnetic QCPs, which supports the spin fluctuation–driven superconductivity. However, the fundamental question remains as to whether a nonmagnetic QCP of electronic nematic order characterized by spontaneous rotational symmetry breaking can promote superconductivity in real materials. Here, we provide an experimental demonstration that a pure nematic QCP exists near the center of a superconducting dome in nonmagnetic FeSe$_{1-x}$ Te$_x$. This result evidences that nematic fluctuations enhanced around the nematic QCP can boost superconductivity.

[1]Present address: Max Planck Institute for Chemical Physics of Solids, 01187 Dresden, Germany.

[2]To whom correspondence may be addressed. Email: ko usuke.ishida@cpfs.mpg.de or shibauchi@k.u-tokyo.ac.jp.

[3]Present address: Department of Applied Physics, University of Tokyo, Tokyo 113-8656, Japan.

[4]Present address: Department of Physics, Tohoku University, Sendai 980-8578, Japan.

temperature without stabilizing the magnetic order, but T_c is found to show an abrupt decrease across the end point of the nematic phase (16). Thus, experimentally, there is no evidence in S-substituted FeSe that nematic fluctuations enhanced at the end point of T_s promote superconductivity.

The Se site of FeSe can also be substituted by isovalent Te. Previously, the single-crystal studies of $FeSe_{1-x} Te_x$ were almost limited to the high Te–composition side ($x \gtrsim 0.50$), which had shown that $FeSe_{0.5} Te_{0.5}$ does not exhibit nematic order with T_c as high as 14 K (17, 18). Although elastoresistivity measurements in $FeSe_{0.4} Te_{0.6}$ single crystals grown by the flux method show that the nematic susceptibility diverges toward ~ -10 K (19, 20), its evolution to FeSe has not been clarified. Recent advances in the single-crystal growth of $FeSe_{1-x} Te_x$ by the flux method under the temperature gradient conditions (21) and the chemical vapor transport (CVT) technique (22) have enabled the systematic tracing of the nematic and superconducting transition temperatures with Te substitution by overcoming the phase separation issue previously reported for $0.10 \lesssim x \lesssim 0.30$ (23). It has been found that T_s of the CVT-grown single crystals is monotonically suppressed with increasing Te concentrations and disappears around $x = 0.50$, whereas T_c first decreases, reaches its minimum at $x \sim 0.30$, and then, turns to increase (22), as reproduced in Fig. 1B, Lower.

The increase in T_c toward the end point of T_s points to a potential link between suppressed nematicity and enhanced super-

conductivity in $FeSe_{1-x} Te_x$. However, this increasing trend of T_c with vanishing T_s stands in marked contrast to the phase diagram of $FeSe_{1-x} S_x$, which raises the fundamental question of the origin of this difference. To discuss the above issues, it is essential to clarify how nematic fluctuations evolve with Te substitutions compared with the S-substitution case and whether we have a nematic QCP in the phase diagram of $FeSe_{1-x} Te_x$. Here, by performing systematic elastoresistivity measurements on $FeSe_{1-x} Te_x$ single crystals to quantify the nematic susceptibility, we demonstrate that $FeSe_{1-x} Te_x$ is an unprecedented system whose nematic QCP lies near the center of the superconducting dome in isolation from any other long-range orders. Comparisons between the results in $FeSe_{1-x} Te_x$ and $FeSe_{1-x} S_x$ imply that the dominance of nematic fluctuations over antiferromagnetic fluctuations is the key to enhancing T_c around the nonmagnetic nematic QCP.

Results

Nematic order is characterized by rotational symmetry breaking, and thus, its order parameter can be expressed by the anisotropy of physical quantities, such as electrical resistivity (5). Since the uniaxial strain works as a conjugate field to the nematic order parameter, the nematic susceptibility above the transition temperature T_s can be obtained from the electronic anisotropy induced by the strain applied to the system as a perturbation. In our elastoresistivity measurements, we assume the in-plane resistivity anisotropy as an order parameter of the nematic phase, and the anisotropic biaxial strain is applied using the piezoelectric device (Materials and Methods) (24). As shown in Fig. 2A, for the resistivity measurements along two directions on a single sample, we apply the Montgomery method to the square-shaped crystals. The samples are directly glued on the surface of the piezo stack, and the strain is controlled by applying the voltage to the device and monitored by the strain gauge attached on the other side.

In the tetragonal FeSe-based materials with the D_{4h} point group, there are two candidates for the in-plane nematic order. One is along the adjacent Fe–chalcogen direction with B_{1g} irreducible representation, and the other is along the Fe–Fe direction with B_{2g} symmetry (here, we use the experimental two-Fe unit cell notation). Nematic susceptibility for each symmetry channel can be measured by applying the strain along its corresponding direction and by using the elastoresistivity tensor defined as $m_{ij} = (\Delta\rho/\rho)_i/\varepsilon_j$, where $(\Delta\rho/\rho)_i$ is the relative change of resistivity against the strain ε_j, with subscripts i and j represented by the Voigt notation ($1 = xx, 2 = yy, 3 = zz, 4 = yz, 5 = zx, 6 = xy$); the B_{1g} and B_{2g} components can be expressed as $m_{11} - m_{12}$ and $2m_{66}$, respectively (19).

Fig. 2B exhibits the temperature dependence of the two nematic susceptibilities for an FeSe single crystal. Above T_s, $2m_{66}$ displays a strong temperature evolution with much larger magnitude compared with $m_{11} - m_{12}$, confirming the B_{2g} Ising nematic order of FeSe. Furthermore, in the disordered state above T_s, $2m_{66}$ obeys the Curie–Weiss law:

$$2m_{66}(T) = \frac{a}{T - T_0} + 2m_{66}^{(0)}, \qquad [1]$$

where a and $2m_{66}^{(0)}$ are temperature-independent constants. The Curie–Weiss temperature T_0 gives the bare nematic transition temperature in the absence of nematoelastic coupling in the system. However, the presence of finite coupling shifts the thermodynamic nematic transition from T_0 to T_s ($> T_0$). Inside the ordered phase below T_s, $2m_{66}(T)$ no longer follows the Curie–Weiss law, as shown in Fig. 2B. The Curie–Weiss temperature dependence of the nematic susceptibility above T_s in FeSe has also
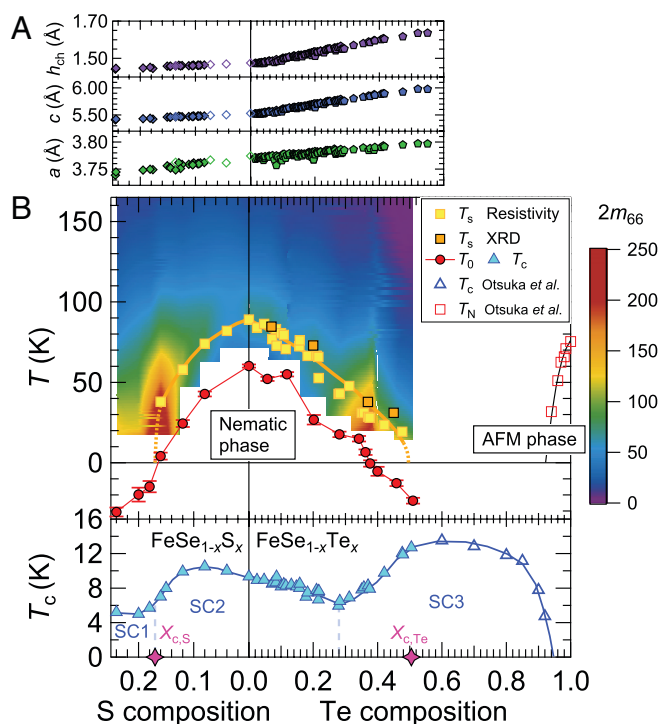

Fig. 1. Nonmagnetic nematic quantum critical points in FeSe-based superconductors. (A) S and Te composition dependence of the a-axis length (Bottom), c-axis length (Middle), and the height of the chalcogen from the Fe plane (Top). Closed pentagons and open diamonds are from refs. 22 and 37, respectively. (B) Combined phase diagram of $FeSe_{1-x} S_x$ and $FeSe_{1-x} Te_x$, which includes T_s determined by the resistivity (yellow squares) and X-ray diffraction experiments (orange squares) (22), T_c (blue triangles), the transition temperature to the antiferromagnetic (AFM) phase T_N (red squares) (31), and T_0 obtained from the analysis of $2m_{66}$ data (red circles). The data of closed symbols are from the single crystals grown by the CVT technique (22), and the data of open symbols in the highly Te substituted region are taken from the study of single crystals synthesized by the flux method (31). The magnitude of $2m_{66}$ is shown as a color plot. T_c has a two-dome structure, which contains two nematic QCPs ($x_{c,S}$ and $x_{c,Te}$), and the superconducting state can be separated into three regions (SC1, SC2, and SC3), whose properties are considered to be different.
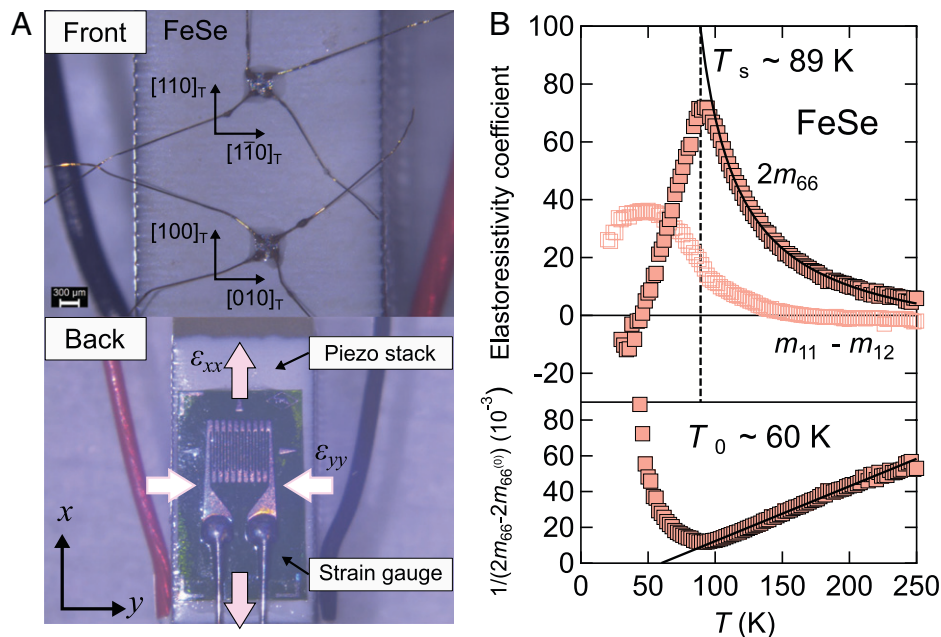
Fig. 2. B_{1g} and B_{2g} nematic susceptibilities of FeSe measured by elastoresistivity technique. (*A*) Photographs of the elastoresistance measurement setup. The square-shaped samples with electric contacts on four corners were directly glued on the piezo stack. On the back side, the strain gauge was attached to measure the amount of the applied strain. For the B_{2g} and B_{1g} nematic susceptibility measurements, the samples are aligned along the $[110]_T$ and $[100]_T$ directions, respectively. *B, Upper* shows the temperature dependence of the two elastoresistivity coefficients of FeSe. The black line represents the Curie–Weiss fit for $2m_{66}(T)$. *B, Lower* displays the inverse of $2m_{66} - 2m_{66}^{(0)}$, where $2m_{66}^{(0)}$ is determined by the Curie–Weiss fitting.

been reported in the previous measurements of the elastoresistivity, Young modulus, and Raman scattering (25–28).

Next, we discuss the evolution of nematic susceptibility with Te substitution. Single crystals of FeSe$_{1-x}$Te$_x$ used in this study were grown by the CVT technique, which can tune the lattice parameters continuously (Fig. 1*A*). The CVT-grown crystals show homogeneous distributions of Te ions (*SI Appendix*, Fig. S1) with no resistivity upturn (22), which is caused by the localization effects due to excess Fe as reported in crystals synthesized by the Bridgman method for $x \gtrsim 0.50$ (20, 29). As depicted in Fig. 3, our systematic measurements in a wide range of Te composition $0 \leq x \leq 0.51$ reveal that with increasing x, the B_{2g} nematic susceptibility $2m_{66}$ exhibits a continuous evolution with a gradual decrease in T_s. For all Te compositions with finite T_s, the temperature dependence of $2m_{66}$ above T_s can be reasonably described by the Curie–Weiss function, evidencing their continuous nematic transitions (*SI Appendix* has the protocol of Curie–Weiss analysis). The Curie–Weiss temperature dependence can be also seen at low temperatures in the tetragonal $x = 0.51$, but here, we find a clear deviation from the Curie–Weiss behavior at high temperatures $T \gtrsim 150$ K. The magnitude of $2m_{66}$ becomes largest at $x = 0.38$, in which the Curie–Weiss temperature becomes $T_0 \sim 0$ K. For comparison, we have also measured the B_{1g} nematic susceptibility $m_{11} - m_{12}$, which is found to be much less significant than $2m_{66}$ even in the tetragonal $x = 0.51$ (*SI Appendix*, Fig. S2), demonstrating that the large signal in $2m_{66}$ solely comes from the B_{2g} nematic response covering the entire Te composition range of the present study. The observed much weaker temperature dependence of $m_{11} - m_{12}$ contrasts with the case of FeTe, in which $m_{11} - m_{12}$ shows a diverging behavior toward the onset temperature of the double-stripe magnetism (30), while $2m_{66}$ is much less temperature dependent (20). This implies that spin fluctuations associated with the double-stripe magnetic order are almost negligible for $x \leq 0.51$.

From the elastoresistivity measurements, we map out the magnitude of $2m_{66}$ in the phase diagram of FeSe$_{1-x}$Te$_x$ (Fig. 1*B*).

The Curie–Weiss temperature T_0 decreases almost monotonically with increasing Te composition and crosses the zero temperature line around $x = 0.38$, where the magnitude of $2m_{66}$ is strongly enhanced. Since there have been no reports for long-range magnetic order up to $x \sim 0.90$ (31), the observed diverging B_{2g} nematic susceptibility toward 0 K evidences if the electron subsystem was not under the lattice environment, we would have the nonmagnetic nematic QCP around $x = 0.38$. Note that the intensity of $2m_{66}$, which measures the dynamic nematic susceptibility, should become strongest at $T_0 \sim 0$ K because it sees the scale of the bare nematic transition temperature (32, 33). The thermodynamic QCP, in which the continuous electronic nematic transition takes place at zero temperature, is shifted to the end point of T_s due to the inevitable finite nematoelastic coupling.

The obtained set of nematic susceptibility data can be compared with the x dependence of T_c, combined with the previous reports for $x \gtrsim 0.60$ (Fig. 1*B*), which clearly indicates that the nematic QCP in this system locates near the center of the superconducting dome. This implies a close correlation between the nematic quantum phase transition and enhanced superconductivity. Our results are consistent with the recent study for the Te-rich side using Bridgman crystals, which shows the smooth suppression of $2m_{66}$ for $x \gtrsim 0.50$ (20).

Our results on FeSe$_{1-x}$Te$_x$ indicate that the isovalent Te substitution for Se, which may be considered as a negative chemical pressure effect (Fig. 1*A*), affects the superconductivity in a completely different way from the S substitution corresponding to a positive chemical pressure. To gain more insights into the difference between the Te and S substitution effects, we also performed the elastoresistivity measurements for FeSe$_{1-x}$S$_x$ in the same experimental setup (*SI Appendix*, Fig. S4) and plotted the intensities of $2m_{66}$ on the same scale with that of FeSe$_{1-x}$Te$_x$ in the combined phase diagram shown in Fig. 1*B*. As previously reported (25), $2m_{66}$ of FeSe$_{1-x}$S$_x$ also follows the Curie–Weiss temperature dependence, and its T_0 changes sign around $x = 0.17$ with a strong enhancement of the magnitude of nematic susceptibility,
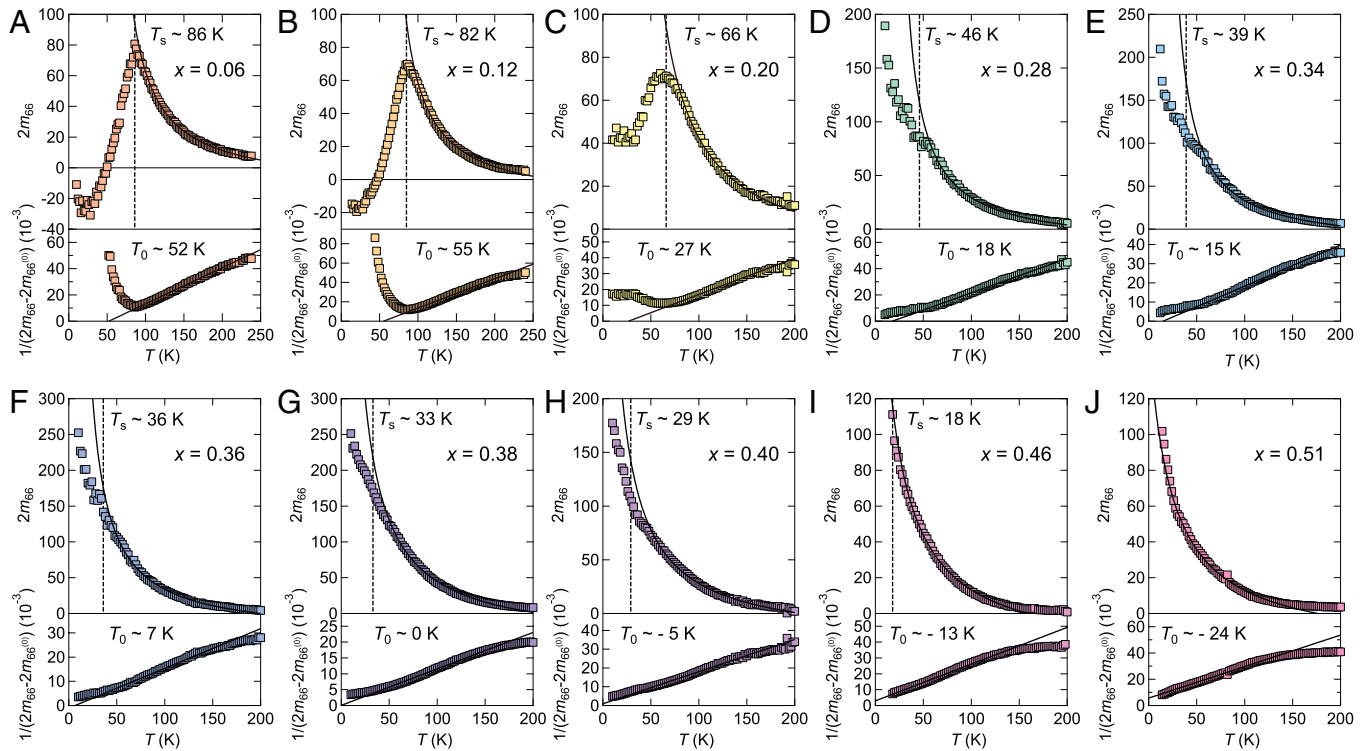
Fig. 3. Evolution of elastoresistivity coefficients $2m_{66}$ in FeSe$_{1-x}$Te$_x$. Temperature dependence of B_{2g} nematic susceptibilities (*Upper*) and their Curie–Weiss analyses (*Lower*) for $x = 0.06$ (*A*), 0.12 (*B*), 0.20 (*C*), 0.28 (*D*), 0.34 (*E*), 0.36 (*F*), 0.38 (*G*), 0.40 (*H*), 0.46 (*I*), and 0.51 (*J*). In each panel, the structural transition temperatures T_s are shown by the vertical dashed lines, except for $x = 0.51$ with no structural transition. Black lines represent the Curie–Weiss fitting, and the obtained Curie–Weiss temperatures T_0 are indicated in *Lower*.

Discussion

Although diverging behavior of $2m_{66}$ around the nematic QCP of FeSe$_{1-x}$S$_x$ is almost identical to that of FeSe$_{1-x}$Te$_x$, T_c of FeSe$_{1-x}$S$_x$ exhibits a sudden decrease across the quantum phase transition, which is in sharp contrast to the superconducting dome in FeSe$_{1-x}$Te$_x$. As illustrated in Fig. 1 *B*, *Lower*, the dependence of T_c on S concentration inside the nematic phase of FeSe$_{1-x}$S$_x$ shows a broad peak structure, which is connected continuously to that in FeSe$_{1-x}$Te$_x$ across $x = 0$ (FeSe), forming a superconducting dome (SC2). In this SC2 region of FeSe$_{1-x}$S$_x$, several bulk probes and surface-sensitive techniques have provided evidence that their superconducting gap structures have strong momentum dependence (14, 34, 35). Recent NMR experiments revealed that antiferromagnetic fluctuations with the (π, π) wave vector are enhanced inside the nematic phase of FeSe$_{1-x}$S$_x$, which appears to be in correspondence with the T_c dome (36). Moreover, high-pressure studies in FeSe$_{1-x}$S$_x$ demonstrated that T_c is enhanced around the end points of the pressure-induced antiferromagnetic phase (37). These results imply the close relationship between antiferromagnetic fluctuations and enhanced superconductivity in the SC2 region.

In FeSe$_{1-x}$Te$_x$, the x dependence of T_c shows a minimum at $x \sim 0.30$, above which another superconducting dome emerges around the nematic QCP found in this study. This nonmonotonic $T_c(x)$ in FeSe$_{1-x}$Te$_x$ strongly suggests that the superconducting state (SC3) in the $x \gtrsim 0.30$ region has a different mechanism from

demonstrating the B_{2g} nematic QCP (*SI Appendix*, Fig. S4). Furthermore, the singular behavior in $2m_{66}$ at the QCP of FeSe$_{1-x}$S$_x$ is found to be quite similar to that of FeSe$_{1-x}$Te$_x$ (Fig. 4*A*), suggesting that the underlying nematic quantum critical behavior is essentially the same between the two systems.

that in SC2. Indeed, the full-gap superconductivity, which is quite different from the strongly momentum-dependent gap structures found in the SC2 region, has been reported by scanning tunneling spectroscopy in optimally substituted FeSe$_{1-x}$Te$_x$ (38). Although Raman spectroscopy revealed that in FeSe$_{0.4}$Te$_{0.6}$, the strength of electron–phonon coupling is insufficient to give $T_c = 14$ K (39), no significant (π, π) antiferromagnetic fluctuations are detected in the NMR experiments (40), which is consistent with the recent high-pressure study in FeSe$_{1-x}$Te$_x$ showing that the pressure-induced antiferromagnetic order fades away above $x \sim 0.14$ (22). These results can preclude that the superconducting dome at $x \gtrsim 0.30$ is associated with magnetic fluctuations and further support that the enhancement of critical temperature
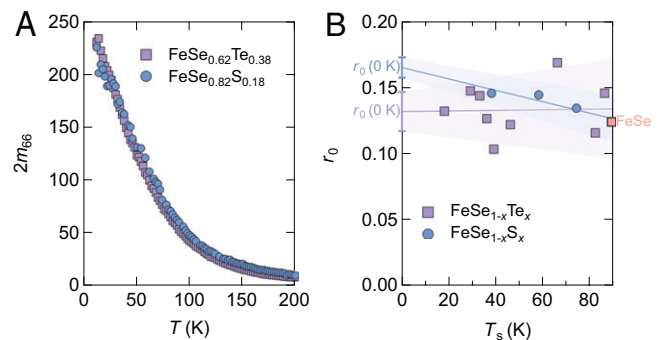

Fig. 4. Similarities of nonmagnetic B_{2g} nematic quantum criticality in FeSe$_{1-x}$Te$_x$ and FeSe$_{1-x}$S$_x$. (*A*) The temperature dependence of $2m_{66}$ for FeSe$_{1-x}$Te$_x$ with $x = 0.38$ (purple squares) from Fig. 3*G* is compared with that for FeSe$_{1-x}$S$_x$ with $x = 0.18$ (blue circles) from *SI Appendix*, Fig. S4*D*. (*B*) Strength of nematoelastic coupling $r_0 = (T_s - T_0)/T_F$ in FeSe (orange square), FeSe$_{1-x}$Te$_x$ (purple squares), and FeSe$_{1-x}$S$_x$ (blue circles) as a function of the structural transition temperature. The purple and blue lines represent the linear fitting for the r_0 values of FeSe$_{1-x}$Te$_x$ and FeSe$_{1-x}$S$_x$, and their shades correspond to the uncertainties of the fitting.

in the SC3 region comes from the nematic quantum critical fluctuations observed in our elastoresistivity measurements.

Although several theories have shown that nematic fluctuations can enhance T_c, most of these theories consider pure electronic systems (8, 9), which do not include the coupling to the underlying lattice inevitably present in real materials. Recently, however, it has been pointed out that this nematoelastic coupling plays a crucial role in the nematic quantum criticality (32). Through the coupling to the lattice, the divergence of the correlation length at the nematic QCP is restricted only along the two high-symmetry regions, and the criticality can be cut off. Consequently, the strength of nematoelastic coupling becomes an important parameter at the nematic QCP, and this is closely related to the parameter $r_0 = (T_s - T_0)/T_F$, where T_F is the Fermi temperature. According to this theory, in FeSe-based materials with small Fermi energy, the effect of nematoelastic coupling can be particularly significant compared with other iron-based superconductors (*SI Appendix, SI Text* and Fig. S6). To compare the strength of the coupling with the lattice in FeSe$_{1-x}$ S$_x$ and FeSe$_{1-x}$ Te$_x$, we plot in Fig. 4B the r_0 parameters estimated from the obtained T_s and T_0 values as a function of structural transition temperature. Here, we assume that the Fermi energy is independent of composition and set to 20 meV for simplicity. We find that r_0 values of these two systems are close to each other, and moreover, their strengths at thermodynamic nematic QCP [$r_0(T_s \to 0)$] are also similar. The almost identical r_0 parameters between FeSe$_{1-x}$ S$_x$ and FeSe$_{1-x}$ Te$_x$ mean that the nematoelastic coupling is equally important to discuss the nematic quantum criticality in both systems.

It has been suggested from recent studies that the absence of the T_c enhancement around the QCP in FeSe$_{1-x}$ S$_x$ is related to this nematoelastic coupling effect (41, 42). However, our above analysis reveals that even in the presence of sizable coupling to the lattice, the superconductivity can be enhanced around the nematic QCP in FeSe$_{1-x}$ Te$_x$. The origin of this distinct difference between FeSe$_{1-x}$ S$_x$ and FeSe$_{1-x}$ Te$_x$ is an intriguing issue that deserves further investigation, but the recent phenomenological theory (33) may offer a qualitative explanation. This theory predicts that the enhancement of T_c near the nematic QCP is expected only when the nematoelastic coupling parameter r_0 is much smaller than the ratio $(U/V)^2$, where U and V are the phenomenological parameters representing the nematic and magnetic pairing interactions, respectively (33). Although our observations of identically diverging nematic susceptibility around the two nematic QCPs (Fig. 4A) and similar strengths of nematoelastic coupling (Fig. 4B) imply that the nematic interaction U and coupling parameter r_0 are similar in FeSe$_{1-x}$ S$_x$ and FeSe$_{1-x}$ Te$_x$, the spin interaction term V is considered quite different between them, as revealed by NMR measurements (36, 40). Namely, FeSe$_{1-x}$ S$_x$ with no enhancement of T_c exhibits relatively strong spin fluctuations, leading to a small $(U/V)^2$ parameter, which may be unable to satisfy the $r_0 \ll (U/V)^2$ relation; however, FeSe$_{1-x}$ Te$_x$, in which no significant antiferromagnetic fluctuations are found and thus, a larger $(U/V)^2$ is expected, exhibits a clear superconducting dome near the thermodynamic nematic QCP.

Before concluding, we point out that the two superconducting domes (SC2 and SC3) studied here may have some similarities with the phase diagram of hole-doped high-T_c cuprate superconductors under high magnetic fields, which also has two peaks in underdoped and slightly overdoped regions (43). While the center of one dome locates near the end point of the short-range antiferromagnetic order, the other with higher T_c is around the critical doping at which the enigmatic pseudogap phase terminates. Recent studies showed that significant electronic anisotropy develops inside the pseudogap phase (44, 45), and there is evidence for

enhanced nematic fluctuations at its critical point (6, 46). This similarity in the systems with quite different electronic structures may imply that nematic fluctuations can enhance superconductivity more strongly than previously thought, which stimulates further investigation.

In summary, the present systematic elastoresistivity measurements in FeSe$_{1-x}$ Te$_x$ single crystals provide strong evidence for the nonmagnetic pure nematic QCP accompanied by the superconducting dome. The enhancement of critical temperature in this material can be ascribed to the quantum critical fluctuations of the electronic nematic phase, which can offer a unique route to high-temperature superconductivity. We note that this is further supported by the recent high-field experiments in FeSe$_{1-x}$ Te$_x$, which have revealed that the superconducting dome straddles the nematic QCP quite robustly even when the dome shrinks by applying the magnetic field (47).

Materials and Methods

Single Crystals. Single crystals of FeSe$_{1-x}$ S$_x$ and FeSe$_{1-x}$ Te$_x$ were grown by the CVT technique (22, 37). The samples of FeSe$_{1-x}$ Te$_x$ measured in this study are from the same batches used in ref. 22. Fe, Se, and S (Te) powders were mixed with AlCl$_3$ and KCl transport agents and sealed in evacuated quartz ample. Temperatures of the source and sink sides were set at 420 °C and 250 °C for FeSe$_{1-x}$ S$_x$ and FeSe$_{1-x}$ Te$_x$ with $x \lesssim 0.25$ and 620 °C and 450 °C for FeSe$_{1-x}$ Te$_x$ with $x \gtrsim 0.25$, respectively.

The actual Te and S compositions were determined for each sample before the elastoresistivity measurements by the c-axis length measured by X-ray diffraction (Fig. 1A). For all the samples, homogeneous distributions of chalcogen ions were confirmed by energy-dispersive X-ray spectroscopy (*SI Appendix*, Fig. S1).

Elastoresistance Measurements. For the systematic measurements of nematic susceptibility, we adopt the elastoresistivity measurement technique using the piezoelectric device. In this technique, we measure the strain-induced in-plane resistivity anisotropy. The experimental setup is shown in Fig. 2A. The samples are cut into square shapes, and the resistivity along the x and y directions (ρ_{xx} and ρ_{yy}) is measured by the Montgomery method. One advantage of this method is that we can measure both ρ_{xx} and ρ_{yy} in a given sample. To discuss the systematic dependence of the magnitude of the nematic susceptibility, we set the lateral sample size approximately fixed to 250×250 μm to minimize the possible size dependence.

After making the electrical contacts on the prepared samples, we glued them on the piezo stacks. The strain was transmitted to the sample via orthorhombic distortion of the device and controlled in situ by applying the voltage to the piezo stack. The amount of the strain ε_{xx} was measured by a strain gauge attached on the backside of the device, and the orthogonal strain ε_{yy} was calculated by the Poisson's ratio of piezo stacks calibrated beforehand.

Data Availability. All study data are included in the article and/or *SI Appendix*.

Author affiliations: ªDepartment of Advanced Materials Science, University of Tokyo, Chiba 277-8561, Japan

Author contributions: K.I. and T.S. designed research; K.I., Y.O., M.T., K. Mukasa, M.Q., M.S., Y.S., K. Matsuura, Y.M., and K.H. performed research; K.I., Y.O., and T.S. analyzed data; and K.I. and T.S. wrote the paper.

The authors declare no competing interest.

This article is a PNAS Direct Submission.

1. S. Sachdev, B. Keimer, Quantum criticality. *Phys. Today* **64**, 29 (2011).
2. N. Mathur *et al.*, Magnetically mediated superconductivity in heavy fermion compounds. *Nature* **394**, 39–43 (1998).
3. T. Shibauchi, A. Carrington, Y. Matsuda, A quantum critical point lying beneath the superconducting dome in iron pnictides. *Annu. Rev. Condens. Matter Phys.* **5**, 113–135 (2014).
4. T. Moriya, K. Ueda, Antiferromagnetic spin fluctuation and superconductivity. *Rep. Prog. Phys.* **66**, 1299 (2003).
5. E. Fradkin, S. A. Kivelson, M. J. Lawler, J. P. Eisenstein, A. P. Mackenzie, Nematic Fermi fluids in condensed matter physics. *Annu. Rev. Condens. Matter Phys.* **1**, 153–178 (2010).
6. K. Ishida *et al.*, Divergent nematic susceptibility near the pseudogap critical point in a cuprate superconductor. *J. Phys. Soc. Jpn.* **89**, 064707 (2020).
7. F. Ronning *et al.*, Electronic in-plane symmetry breaking at field-tuned quantum criticality in CeRhIn$_5$. *Nature* **548**, 313–317 (2017).
8. S. Lederer, Y. Schattner, E. Berg, S. A. Kivelson, Enhancement of superconductivity near a nematic quantum critical point. *Phys. Rev. Lett.* **114**, 097001 (2015).
9. T. A. Maier, D. J. Scalapino, Pairing interaction near a nematic quantum critical point of a three-band CuO$_2$ model. *Phys. Rev. B.* **90**, 174510 (2014).
10. S. Lederer, Y. Schattner, E. Berg, S. A. Kivelson, Superconductivity and non-Fermi liquid behavior near a nematic quantum critical point. *Proc. Natl. Acad. Sci. USA* **114**, 4905–4910 (2017).
11. C. Eckberg *et al.*, Sixfold enhancement of superconductivity in a tunable electronic nematic system. *Nat. Phys.* **16**, 346–350 (2020).
12. P. Malinowski *et al.*, Suppression of superconductivity by anisotropic strain near a nematic quantum critical point. *Nat. Phys.* **16**, 1189–1193 (2020).
13. S. Lederer, E. Berg, E. A. Kim, Tests of nematic-mediated superconductivity applied to ba$_{1-x}$sr$_x$ni$_2$as$_2$. *Phys. Rev. Res.* **2**, 023122 (2020).
14. T. Shibauchi, T. Hanaguri, Y. Matsuda, Exotic superconducting states in FeSe-based materials. *J. Phys. Soc. Jpn.* **89**, 102002 (2020).
15. J. P. Sun *et al.*, Dome-shaped magnetic order competing with high-temperature superconductivity at high pressures in FeSe. *Nat. Commun.* **7**, 12146 (2016).
16. P. Reiss *et al.*, Suppression of electronic correlations by chemical pressure from FeSe to FeS. *Phys. Rev. B.* **96**, 121103(R) (2017).
17. S. Li *et al.*, First-order magnetic and structural phase transitions in Fe$_{1+y}$Se$_x$Te$_{1-x}$. *Phys. Rev. B.* **79**, 054503 (2009).
18. B. C. Sales *et al.*, Bulk superconductivity at 14 K in single crystals of Fe$_{1+y}$Te$_x$ Se$_{1-x}$. *Phys. Rev. B.* **79**, 094521 (2009).
19. H. H. Kuo, J. H. Chu, J. C. Palmstrom, S. A. Kivelson, I. R. Fisher, Ubiquitous signatures of nematic quantum criticality in optimally doped Fe-based superconductors. *Science* **352**, 958–962 (2016).
20. Q. Jiang *et al.*, Nematic fluctuations in an orbital selective superconductor Fe$_{1+y}$Te$_{1-x}$Se$_x$. arXiv [Preprint] (2020). https://arxiv.org/abs/2006.15887 (Accessed 6 April 2022).
21. K. Terao, T. Kashiwagi, T. Shizu, R. A. Klemm, K. Kadowaki, Superconducting and tetragonal-to-orthorhombic transitions in single crystals of FeSe$_{1-x}$Te$_x$ ($0 \leq x \leq 0.61$). *Phys. Rev. B.* **100**, 224516 (2019).
22. K. Mukasa *et al.*, High-pressure phase diagrams of FeSe$_{1-x}$Te$_x$: Correlation between suppressed nematicity and enhanced superconductivity. *Nat. Commun.* **12**, 381 (2021).
23. M. Fang *et al.*, Superconductivity close to magnetic instability in Fe(Se$_{1-x}$Te$_x$)$_{0.82}$. *Phys. Rev. B.* **78**, 224503 (2008).
24. J. H. Chu, H. H. Kuo, J. G. Analytis, I. R. Fisher, Divergent nematic susceptibility in an iron arsenide superconductor. *Science* **337**, 710–712 (2012).
25. S. Hosoi *et al.*, Nematic quantum critical point without magnetism in FeSe$_{1-x}$S$_x$ superconductors. *Proc. Natl. Acad. Sci. USA.* **113**, 8139–8143 (2016).
26. M. A. Tanatar *et al.*, Origin of the resistivity anisotropy in the nematic phase of FeSe. *Phys. Rev. Lett.* **117**, 127001 (2016).
27. A Böhmer *et al.*, Origin of the tetragonal-to-orthorhombic phase transition in FeSe: A combined thermodynamic and NMR study of nematicity. *Phys. Rev. Lett.* **114**, 027001 (2015).
28. P. Massat *et al.*, Charge-induced nematicity in FeSe. *Proc. Natl. Acad. Sci. USA.* **113**, 9177–9181 (2016).
29. Y. Sun, Z. Shi, T. Tamegai, Review of annealing effects and superconductivity in Fe$_{1+y}$Te$_{1-x}$Se$_x$ superconductors. *Supercond. Sci. Technol.* **32**, 103001 (2019).
30. W. Bao *et al.*, Tunable ($\delta\pi$, $\delta\pi$)-type antiferromagnetic order in α-Fe(Te,Se) superconductors. *Phys. Rev. Lett.* **102**, 247001 (2009).
31. T. Otsuka *et al.*, Incoherent-coherent crossover and the pseudogap in Te-annealed superconducting Fe$_{1+y}$Te$_{1-x}$Se$_x$ revealed by magnetotransport measurements. *Phys. Rev. B.* **99**, 184505 (2019).
32. I. Paul, M. Garst, Lattice effects on nematic quantum criticality in metals. *Phys. Rev. Lett.* **118**, 227601 (2017).
33. D. Labat, I. Paul, Pairing instability near a lattice-influenced nematic quantum critical point. *Phys. Rev. B.* **96**, 195146 (2017).
34. Y. Sato *et al.*, Abrupt change of the superconducting gap structure at the nematic critical point in FeSe$_{1-x}$S$_x$. *Proc. Natl. Acad. Sci. USA* **115**, 1227–1231 (2018).
35. T. Hanaguri *et al.*, Two distinct superconducting pairing states divided by the nematic end point in FeSe$_{1-x}$S$_x$. *Sci. Adv.* **4**, eaar6419 (2018).
36. P. Wiecki *et al.*, Persistent correlation between superconductivity and antiferromagnetic fluctuations near a nematic quantum critical point in FeSe$_{1-x}$S$_x$. *Phys. Rev. B.* **98**, 020507(R) (2018).
37. K. Matsuura *et al.*, Maximizing T_c by tuning nematicity and magnetism in FeSe$_{1-x}$S$_x$ superconductors. *Nat. Commun.* **8**, 1143 (2017).
38. T. Hanaguri, S. Niitaka, K. Kuroki, H. Takagi, Unconventional *s*-wave superconductivity in Fe(Se,Te). *Science* **328**, 474–476 (2010).
39. S. F. Wu *et al.*, Superconductivity and phonon self-energy effects in Fe$_{1+y}$Te$_{0.6}$Se$_{0.4}$. *Phys. Rev. Res.* **2**, 013373 (2020).
40. D. Arčon *et al.*, Coexistence of localized and itinerant electronic states in the multiband iron-based superconductor FeSe$_{0.42}$Te$_{0.58}$. *Phys. Rev. B.* **82**, 140508(R) (2010).
41. S. Chibani *et al.*, Lattice-shifted nematic quantum critical point in FeSe$_{1-x}$S$_x$. *npj Quantum Mater.* **6**, 37 (2021).
42. P. Reiss *et al.*, Quenched nematic criticality and two superconducting domes in an iron-based superconductor. *Nat. Phys.* **16**, 89–94 (2020).
43. B. J. Ramshaw *et al.*, Quasiparticle mass enhancement approaching optimal doping in a high-T_c superconductor. *Science* **348**, 317–320 (2015).
44. R. Daou *et al.*, Broken rotational symmetry in the pseudogap phase of a high-T_c superconductor. *Nature* **463**, 519–522 (2010).
45. M. J. Lawler *et al.*, Intra-unit-cell electronic nematicity of the high-T_c copper-oxide pseudogap states. *Nature* **466**, 347–351 (2010).
46. N. Auvray *et al.*, Nematic fluctuations in the cuprate superconductor Bi$_2$Sr$_2$CaCu$_2$O$_{8+\delta}$. *Nat. Commun.* **10**, 5209 (2019).
47. K. Mukasa *et al.*, Enhanced superconducting pairing strength near a nonmagnetic nematic quantum critical point. arXiv [Preprint] (2022). https://arxiv.org/abs/2202.11657 (Accessed 6 April 2022).